Plasma Physics

Ionization instability and stable region in potassium seeded argon gas plasma MHD generation

To cite this article: K Yoshikawa and I Michiyoshi 1974 *Plasma Physics* **16** 1085

Plasma Physics, Vol. 16, pp. 1085 to 1099. Pergamon Press 1974. Printed in Northern Ireland

IONIZATION INSTABILITY AND STABLE REGION IN POTASSIUM SEEDED ARGON GAS PLASMA MHD GENERATION

K. YOSHIKAWA
Institute of Atomic Energy, Kyoto Univ., Gokasho, Uji, Japan

and

I. MICHIYOSHI
Department of Nuclear Eng., Kyoto Univ., Yoshida, Kyoto, Japan

(*Received* 4 *June* 1973; *and in final form* 28 *February* 1974)

Abstract—In nonequilibrium MHD generation with alkali metal seeded noble gas plasma, stable regions free from ionization instability are investigated in terms of seed fraction, magnetic field strength and current density by using linear perturbation theory with allowance for the ionization of noble gas atoms. Regardless of fluctuations, a Faraday-type MHD generator with finely segmented electrodes operating with a seed fraction of 10^{-3} gives, in general, higher power density than a smaller seed fraction of 10^{-5}, and the power density can attain the target power density 50 MW/m^3 even at a low gas temperature of 1500°K and a high pressure of 20 atm.

1. INTRODUCTION

IT HAS been pointed out by many authors (KERREBROCK, 1964; BREDERLOW *et al.*, 1966; LOUIS, 1967) that there are obstacles to the realization of an effective nonequilibrium ionization during closed cycle plasma MHD generation; one of the main obstacles now under discussion is the occurrence of ionization instability which results in a large reduction of effective electrical conductivity and Hall parameters, and thus leads to serious deterioration of MHD generator performance. Recently, NAKAMURA *et al.* (1971) proved experimentally that plasma with a fully ionized seed can be used successfully for damping the ionization instability, and showed that the effective electrical conductivity with small seed fractions can be larger than that for high seed fractions under conditions of constant electric field and weak magnetic field. However, since the current density in the stable region in the case of such small seed fractions is severely restricted, as will be shown later, the desired power density can hardly be obtained and remains at a generally low level. This restriction is, of course, very disadvantageous for practical MHD generation. Furthermore, it is very important to know the influence of the operating pressure on the performance of the MHD generator, since in the future practical MHD generation will be performed at appreciably high pressures with HTGR'S.

2. EQUATIONS

The plasma is assumed to be spatially uniform in the initial state, and a perturbation Y' of plasma parameters, such as electron temperature and number density, is assumed to occur in the form of a plane wave whose direction of propagation makes an angle θ with the average current density j (see Fig. 1). The perturbation is assumed to have the form

$$Y' \propto \exp(i\omega t), \tag{1}$$

where ω is a complex angular velocity defined by

$$\omega = \omega_r - i\omega_i. \tag{2}$$

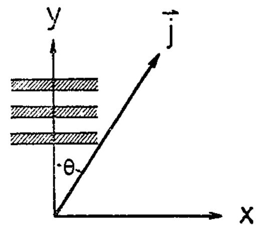

FIG. 1.—Wave pattern of ionization instability.

The maximum growth rate ω_i at angle θ can be obtained in a well known form from linear perturbation theory (KERREBROCK, 1964; NAKAMURA *et al.*, 1971) in which instantaneous Saha equilibrium is assumed and terms apart from the elastic collision loss term neglected in the electron energy equation. In the calculation of the electron collision frequency, Coulomb collisions were included and Ovcharenko's expression (NELSON *et al.*, 1969) used for the cross-section of electrons and argon atoms.

The results of the linear perturbation theory are summarized below.

$$\omega_i = \{\sqrt{(\beta_e n_T)^2 + \sigma_T^2} - \sqrt{(\beta_{cr} n_T)^2 + \sigma_T^2}\}/\tau^*, \tag{3}$$

$$\theta = \arctan\{(1 + \sqrt{1 + \gamma_e^2})/\gamma_e\}, \tag{4}$$

$$\tau^* = n_e\{3kT_e/2 + n_T(3kT_e/2 + e\langle V_i\rangle)\}/(j^2/\sigma), \tag{5}$$

$$\beta_e = eB/m_e \sum_j \nu_{ej} \tag{6}$$

$$\sigma = n_e e^2/m_e \sum_j \nu_{ej}, \tag{7}$$

$$n_T = \mathrm{d}\ln n_e/\mathrm{d}\ln T_e, \tag{8}$$

$$\sigma_T = \mathrm{d}\ln \sigma/\mathrm{d}\ln T_e, \tag{9}$$

$$A_T = \mathrm{d}\ln A/\mathrm{d}\ln T_e, \tag{10}$$

$$\beta_{cr} = \sqrt{A_T^2 - \sigma_T^2}/n_T, \tag{11}$$

$$\gamma_e = \beta_e n_T/\sigma_T, \tag{12}$$

$$A = 3/2 \,.\, kn_e(T_e - T_g)\sum_j (m_e/m_j)\nu_{ej}\,\delta_j, \tag{13}$$

$$e\langle V_i\rangle = e\sum_j n_j^+ V_{ij}/\sum_j n_j^+, \tag{14}$$

$$j = \sqrt{\sigma A}, \tag{15}$$

where n_e, T_e, σ and β_e are electron number density, electron temperature, electrical conductivity and Hall parameter, respectively and β_{cr}, n_j, n_j^+ and A, critical Hall parameter, number density of the jth component, ion number density of the jth component and elastic collision loss of electrons, respectively, and m_j, δ_j, ν_{ej}, $e\langle V_i\rangle$ and eV_{ij} being the mass of the jth component, collision loss parameter of electrons with the jth component, collision frequency of electrons with the jth component, averaged ionization energy and ionization energy of the jth component, respectively.

Considering the ionization of all components, n_T is given by

$$n_T = \sum_j \alpha_j n_j (1 - \alpha_j)(3/2 + eV_{ij}/kT_e) / \sum_j \alpha_j n_j (2 - \alpha_j), \tag{16}$$

where α_j is the degree of ionization defined by the ratio of the jth ion number density to its initial neutral number density.

The performance of a Faraday-type MHD generator with very finely segmented electrodes, each connected to a load resistance R_L, can be obtained from the following simultaneous equations (see Fig. 2).

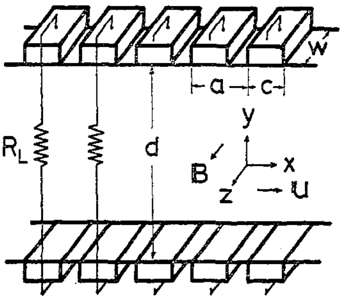

FIG. 2.—Configuration of a Faraday-type MHD generator with finely segmented electrodes.

Current density;

$$\begin{cases} j = \sigma_{\text{eff}} uB/(1 + \sigma_{\text{eff}}/\sigma_L), & \text{(Ohm's law)}, \quad (17) \\ j = (\sigma_{\text{eff}} A)^{1/2}, & \text{(energy equation)}. \quad (18) \end{cases}$$

Power density;

$$P_e = (jS)^2 R_L / Sd = j^2/\sigma_L, \tag{19}$$

where the effective electrical conductivity is assumed to be

$$\sigma_{\text{eff}} = \begin{cases} \sigma & (\beta_e \leqq \alpha_c \beta_{cr}), \quad (20) \\ \alpha_c \sigma \beta_{cr} / \beta_e & (\beta_e \geqq \alpha_c \beta_{cr}). \quad (21) \end{cases}$$

Here α_c is a constant and the load resistance R_L is expressed in terms of σ_L as

$$\sigma_L = d/(SR_L). \tag{22}$$

The expression for σ_{eff} in equation (21) will be discussed later.

3. RESULTS OF CALCULATIONS

Calculations were performed for argon–potassium plasma for a gas temperature of 2000°K. The dependences of electron number density n_e and electrical conductivity σ on the electron temperature T_e, including the effect of the argon ionization, are shown in Fig. 3. It is obvious from the figure that the almost complete ionization of

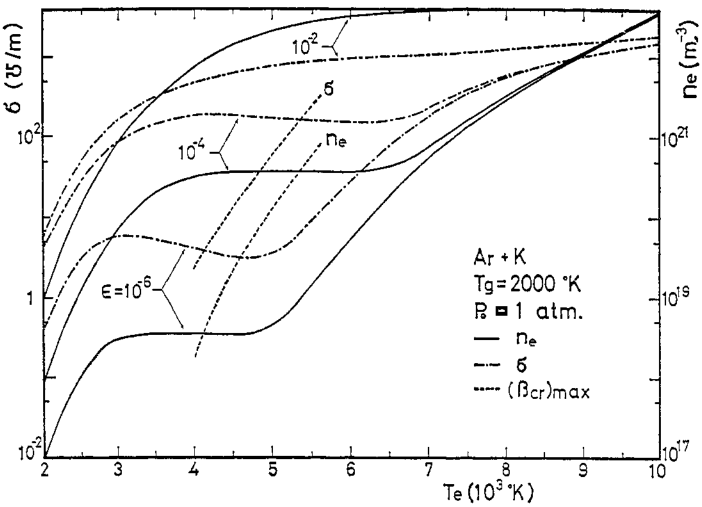

FIG. 3.—Electrical conductivity and electron number density vs electron temperature.

potassium atoms is reached and that the electron number density saturates in the region near the intersection with the dotted line, corresponding to the maximum critical Hall parameter $(\beta_{cr})_{max}$, with increasing electron temperature the argon plays an important rôle in the ionization and the electron number density again sharply increases. The electrical conductivity also at first increases with increasing electron temperature until the region of full ionization of potassium is reached, and then begins to decrease in spite of the temperature rise due to the constant electron density and the increase of electron collision frequency for the relatively smaller seed fractions. When the electron temperature increases further, the electrical conductivity again begins to increase with the onset of argon ionization.

In Fig. 4 the current density j vs electron temperature T_e is shown for various

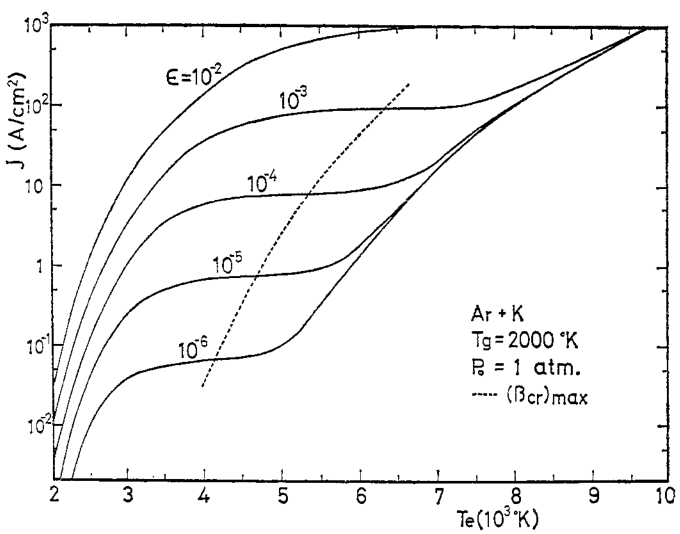

FIG. 4.—Current density vs electron temperature.

seed fractions. Since the current density is roughly proportional to n_e, the plateau seen in Fig. 3 due to small n_T also occurs in Fig. 4.

Critical Hall parameters β_{cr} and electrical conductivity σ vs current densities are shown in Fig. 5. Since the ionization of argon atoms is allowed, the maximum critical Hall parameter does not become infinite but remains finite (NAKAMURA *et al.*, 1971). According to the results obtained, the maximum critical Hall parameter is reached at the minimum value of n_T. It is generally true that the smaller the seed fraction, the larger is the maximum critical Hall parameter and also the lower the corresponding

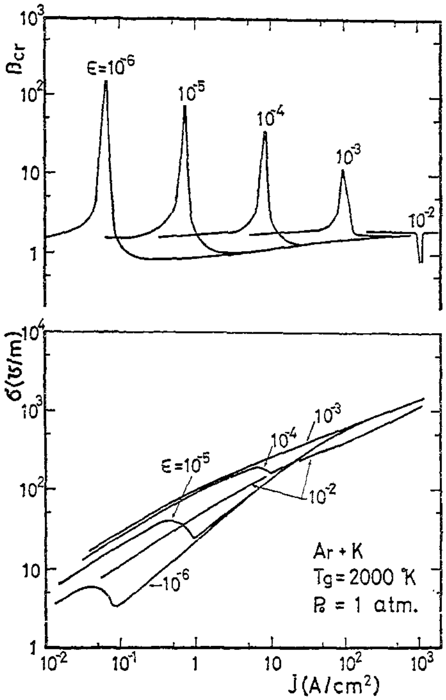

FIG. 5.—Critical Hall parameter and electrical conductivity vs current density.

current density. The peculiar tendency seen for a seed fraction $\varepsilon = 10^{-2}$ near $j = 10^3$ A/cm² is attributed to the fact that the growth rate ω_i essentially cannot be negative under these conditions. The reason why the electrical conductivity decreases after reaching its maximum value is same as that mentioned for Fig. 3. It should be noted that the critical Hall parameter $\beta_{cr} \simeq 2$ obtained experimentally (DETHLEFSEN *et al.*, 1966; BREDERLOW *et al.*, 1966) in the current region of $j = 1$–10 A/cm² for $\varepsilon = 2{\cdot}10^{-3}$ agrees well with that for $\varepsilon = 10^{-3}$ in Fig. 5.

The growth rate ω_i vs the electron temperature T_e at $B = 1$ T is shown in Fig. 6 for various seed fractions. The growth rate ω_i is required only to be negative for the condition of stability, but the absolute value of ω_i is desired to be as large as possible for a rapid decay of the perturbation. Under the present conditions, ω_i is of the order of 10^6 sec^{-1} and hence the system may be regarded as being completely stable simply if ω_i is negative.

Hall parameters β_e and critical Hall parameters β_{cr} vs the electron temperature T_e are shown in Figs. 7 and 8 for $\varepsilon = 10^{-3}$ and 10^{-5}, respectively. Needless to say

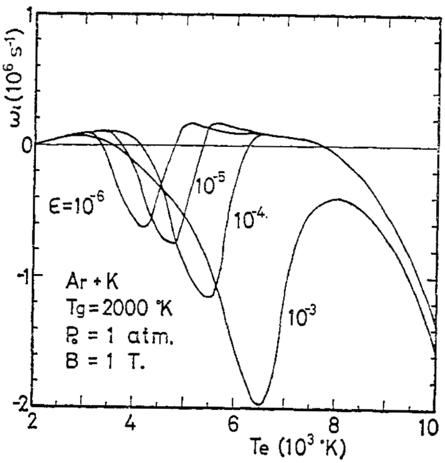

FIG. 6.—Growth rate vs electron temperature.

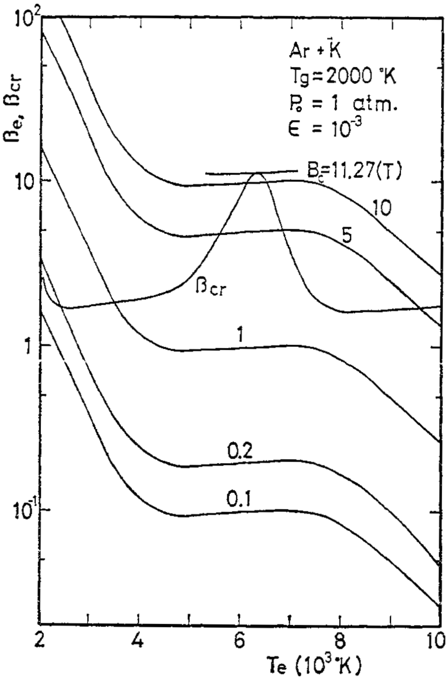

FIG. 7.—Hall parameter and critical Hall parameter vs electron temperature for $\varepsilon = 10^{-3}$.

the system is inherently stable at $T_e = T_g$ independent of the magnetic field strength. In Fig. 7 for $\varepsilon = 10^{-3}$, the system is stable at $B = 0{\cdot}1$ T for all electron temperatures below 10^4°K. However, with the magnetic field increased above $B_c = 11{\cdot}27$ T, the system can no longer be stable at electron temperatures below 10^4°K. This can also be seen in Fig. 8 for $\varepsilon = 10^{-5}$ at magnetic fields above $B_c = 15{\cdot}28$ T, where B_c is the critical magnetic field strength at which the system changes from a stable to an

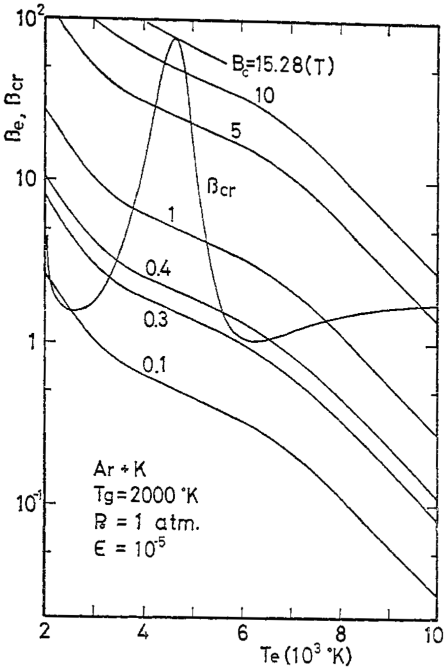

FIG. 8.—Hall parameter and critical Hall parameter vs electron temperature for $\varepsilon = 10^{-5}$.

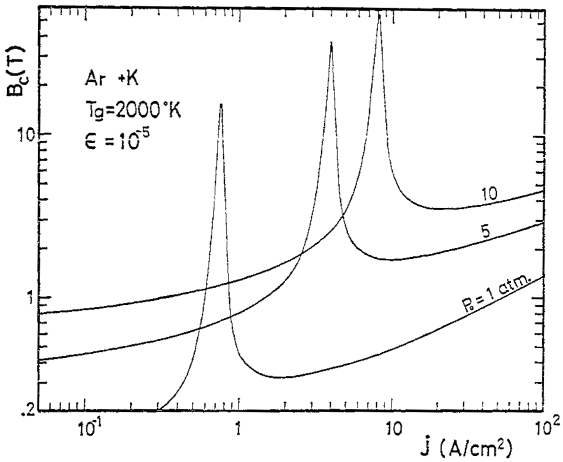

FIG. 9.—Critical magnetic field strength vs current density for various pressures in case of $\varepsilon = 10^{-5}$.

unstable condition. Alteration of the system between stable and unstable states, in general, is seen as the electron temperature is increased at a given field strength.

Figure 9 shows the critical magnetic field strength B_c vs current densities for various pressures in the case $\varepsilon = 10^{-5}$. It is seen that in general B_c becomes large when the pressure is high except in the neighborhood of its maximum, and also that the current density corresponding to the maximum B_c shifts to higher values. As far as the operation mode is concerned, the figures show that MHD generation in the stable mode at a given but weaker magnetic field, say about 5 T, and also at a useful current density may be realized by adjusting the operating pressure.

Stable regions as a function of the magnetic field and current density for various seed fractions at atmospheric pressure are shown in Fig. 10. The regions above and below the curve are unstable and stable, respectively. At a fixed magnetic field the

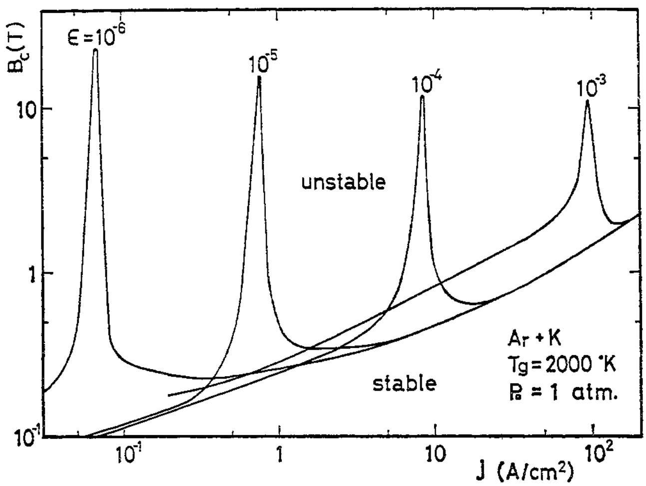

FIG. 10.—Stable regions as a function of magnetic field and current density at atmospheric pressure.

range of current density within which the system is stable is wider for larger seed fractions. At a fixed current density, on the other hand, in the region above $B = 5$ T, the range of the seed fraction for which the system is stable is so narrowly restricted that MHD operation in the stable region does not appear to be very easy.

In Fig. 11 the dependence of the stable region on current density and seed fraction

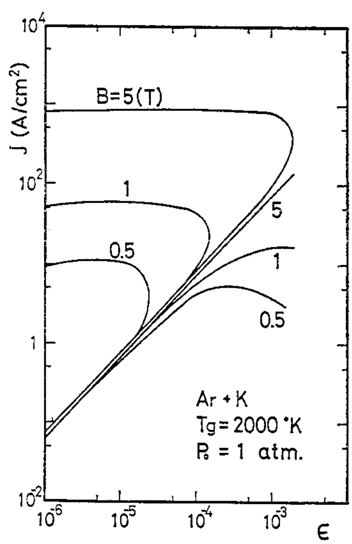

FIG. 11.—Stable regions as a function of current density and seed fraction at atmospheric pressure.

is shown. The region between the upper and lower curves is stable, and current densities of 1–10^2 A/cm^2 correspond approximately to seed fractions of 10^{-5}–10^{-3}. Notice that the linear part of the stable region persists even though the magnetic field is further increased.

The electrical characteristics of a Faraday-type MHD generator with infinitely segmented electrodes, each connected to an individual load resistance R_L as shown in Fig. 2, were calculated for argon–potassium plasma at a gas temperature of 2000°K assuming α_c in equation (21) to be unity. Under these conditions the electrical characteristics of the MHD generator were investigated for seed fractions $\varepsilon = 10^{-5}$

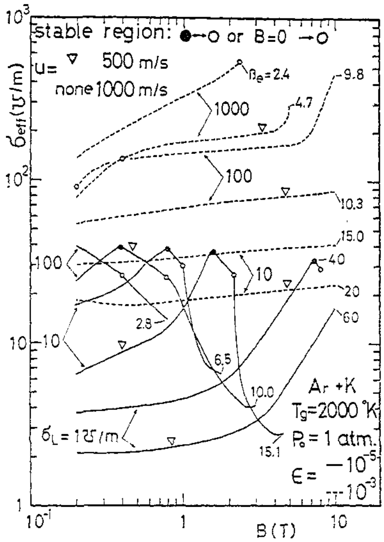

FIG. 12.—Effective electrical conductivity vs magnetic field strength at atmospheric pressure in a Faraday-type MHD generator with finely segmented electrodes.

and 10^{-3} and flow velocities $u = 500$ and 1000 m/sec. According to the experimental results recently obtained by BREDERLOW *et al.* (1973), the expression for the effective electrical conductivity given by equation (21) at $\alpha_c = 1$ shows very good agreement with the experimental results for Ar + 0·05%K at $T_g = 1800$°K in the range of $P_0 =$ 2·1–8·2 bar and $B = 1·1$–3·55 T ($\beta_e \leqq 10·1$). However, they do not mention whether this equation will still rigorously hold good for different seed fractions and gas temperatures. If we assume that equation (21) holds exactly as long as the Hall parameter lies below 10, then no exact comparison for the cases of $\varepsilon = 10^{-5}$, $\sigma_L = 1$ ℧/m or $\varepsilon = 10^{-3}$, $\sigma_L = 10$ ℧/m can be made, as for these cases β_e exceeds 10 at large magnetic field strengths (Figs. 12–14).

In Fig. 17, however, the Hall parameter lies in the range far smaller than $\beta_e = 10$ although the seed fraction is twice as large and the gas temperature 200°K higher than the conditions used by BREDERLOW *et al.* (1973), and thus the equation may be used in this case to estimate the electrical performance for MHD generation. The expression for the effective electrical conductivity from equation (21) at $\alpha_c = 1$ will be more exactly applicable to the actual case of high pressures, since the electron mobility decreases with increasing pressure. In calculating the electrical performance for MHD generation hereafter, equation (21) with $\alpha_c = 1$ will be used as the most reliable

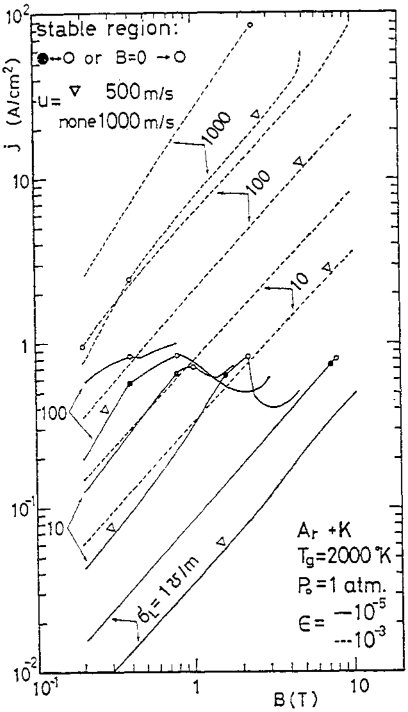

FIG. 13.—Current density vs magnetic field strength at atmospheric pressure in a Faraday-type MHD generator with finely segmented electrodes.

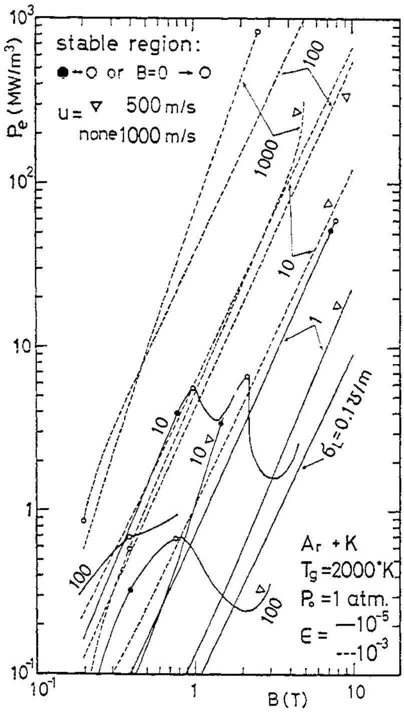

FIG. 14.—Power density vs magnetic field strength at atmospheric pressure in a Faraday-type MHD generator with finely segmented electrodes.

expression presently available for the effective electrical conductivity. It goes without saying that the final conclusion may be slightly altered if other relations which have been proposed (SOLBES, 1968; RIEDMULLER, 1973) were used in place of equation (21), but the major conclusions obtained in this calculation seem to remain valid even for those relations.

The effective electrical conductivity σ_{eff} vs the magnetic field strength B at atmospheric pressure is shown in Fig. 12. In case $\varepsilon = 10^{-5}$ the current density corresponding to the maximum critical Hall parameter is easily reached, hence the largest effective electrical conductivity is realized in the stable region, and with increasing magnetic field σ_{eff} decreases slowly in the stable region and sharply in the unstable region. This tendency is seen also for any σ_L, and the maximum effective electrical conductivity for each σ_L is thus approximately the same at about $\sigma_{eff} \cong 40$ ℧/m. On the other hand, for $\varepsilon = 10^{-3}$, since the electron mobility is small compared with that for $\varepsilon = 10^{-5}$, the stable region still exists in the case when both σ_L and the velocity are large. In this region the increase of the magnetic field causes an immediate increase in the current density resulting in a rise in electron temperature, so that the effective electrical conductivities increase. The obvious difference between $\varepsilon = 10^{-5}$ and 10^{-3} is that in the latter case σ_{eff} increases monotonically regardless of the system condition. When σ_L and the magnetic field strength are suitably fixed, there may be such a case that the effective electrical conductivity for $\varepsilon = 10^{-5}$ is larger than for $\varepsilon = 10^{-3}$, but, in general, they are larger for $\varepsilon = 10^{-3}$ than for $\varepsilon = 10^{-5}$ despite the partial ionization and being subject to the ionization instability in the former case. It may be noted that the electron temperature rise for large σ_L is very rapid even in the region of weak magnetic field strengths due to the strong Joule heating.

The current density vs the magnetic field strength is shown in Fig. 13. In case $\varepsilon = 10^{-5}$ the maximum current density corresponds to the lowest effective electrical conductivity in the stable region, and in the unstable region, except close to the stable region, the current density is roughly proportional to the magnetic field; this applies also to the case $\varepsilon = 10^{-3}$. In general, current densities for $\varepsilon = 10^{-3}$ as well as the effective electrical conductivity seem larger than those for $\varepsilon = 10^{-5}$.

In Fig. 14 the power density variation with the magnetic field strength is shown. At weak magnetic fields power densities for $\varepsilon = 10^{-5}$ are comparable to those for $\varepsilon = 10^{-3}$, but in the region above $B = 1$ T those for $\varepsilon = 10^{-3}$ are obviously far larger resulting in superior operation at a relatively high seed fraction, for example 10^{-3}, provided the relation expressed by equation (21) holds exactly. It should be noted that the power density is still roughly proportional to the square of the magnetic field strength for $\varepsilon = 10^{-3}$ in spite of being in the unstable region. It would be desirable to compare maximum power densities for different seed fractions with each other, but since the power density is a very complicated function of the external load resistance, it is not so easy, in the sense of calculation time, to find the maximum power density. However, in the case of nonequilibrium MHD generation including effects of the ionization instability the maximum power density is expected to appear in the region of $K_{eff} < 0{\cdot}5$, where K_{eff} is an effective load factor defined by $K_{eff} = (1 + \sigma_L/\sigma_{eff})^{-1}$.

As far as the actual MHD generation is concerned, it is of great interest to know the influence of operating pressure and gas temperature on the MHD electrical performance.

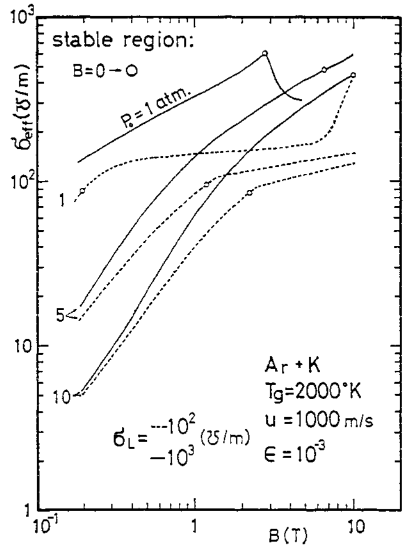

FIG. 15.—Effective electrical conductivity vs magnetic field strength for $\varepsilon = 10^{-3}$ in a Faraday-type MHD generator with finely segmented electrodes.

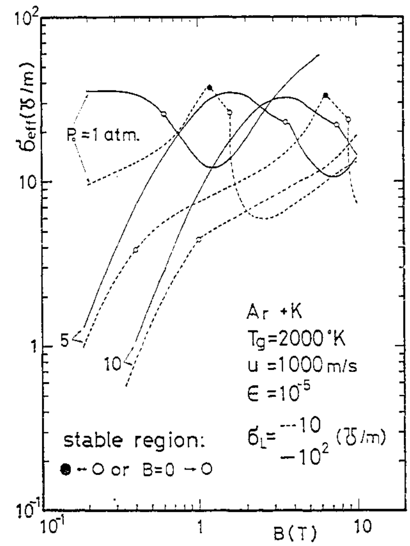

FIG. 16.—Effective electrical conductivity vs magnetic field strength for $\varepsilon = 10^{-5}$ in a Faraday-type MHD generator with finely segmented electrodes.

In Figs. 15 and 16 the effective electrical conductivity σ_{eff} vs the magnetic field strength B is shown for various pressures at $T_g = 2000°\text{K}$ for $\varepsilon = 10^{-3}$ and 10^{-5}, respectively. It is seen from Fig. 15 that σ_{eff} does not depend remarkably on the operating pressure when the magnetic field strength increases, and this tendency will be favorable to practical MHD generation. In the case of $\varepsilon = 10^{-5}$ in Fig. 16, σ_{eff} has a similar shape at higher pressures to that at $P_0 = 1$ atm shifted to the stronger magnetic field. Since the current density which gives $(\beta_{cr})_{\max}$ may be easily realized below $B = 10$ T at the small seed fraction, σ_{eff} becomes a more complicated function of B and σ_L than that for $\varepsilon = 10^{-3}$. A specific magnetic field strength which gives $(\sigma_{eff})_{max}$ at high pressures also exist as in Fig. 12, and this tendency differs apparently in that $(\sigma_{eff})_{max}$ for $\varepsilon = 10^{-3}$ may be obtained in general at the largest B.

In Fig. 17 power densities P_e vs magnetic field strengths B for various pressures P_0 for $\varepsilon = 10^{-3}$ are shown. It is obvious that the power densities scarcely change with the operating pressure and are still proportional to the square of the magnetic field.

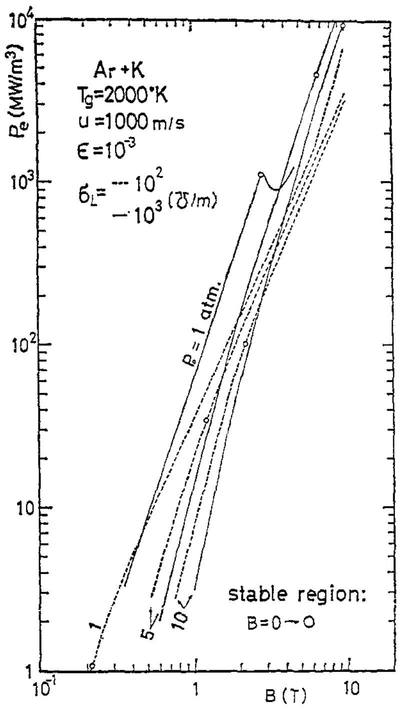

FIG. 17.—Power density vs magnetic field strength for $\varepsilon = 10^{-3}$ and $T_g = 2000$°K for various pressures.

According to this figure, power densities above 50 MW/m^3, which is the present target power density for future practical MHD generation, seem to be very easily obtained even at high pressures for the conditions $T_g = 2000$°K and $u = 1000$ m/sec.

In Figs. 18 and 19 power densities P_e vs magnetic field strengths B and $[P_e/(uB)^2]$ vs B are shown at $T_g = 1500$°K, respectively. Compared with that in Fig. 17 at $T_g = 2000$°K, P_e at $T_g = 1500$°K does not differ as much and shows a similar tendency to that in Fig. 17. It seems that even with a lower gas temperature of 1500°K, power densities more than 50 MW/m^3 are still easily attainable at practical pressures.

In Fig. 19 $[P_e/(uB)^2]$ vs B is shown for various seed fractions at a pressure of 20 atm. These figures obviously show the superiority of operating at higher seed fractions and also afford the feasibility of closed cycle MHD generation which will be used at considerable pressures in connection with HTGR in the future.

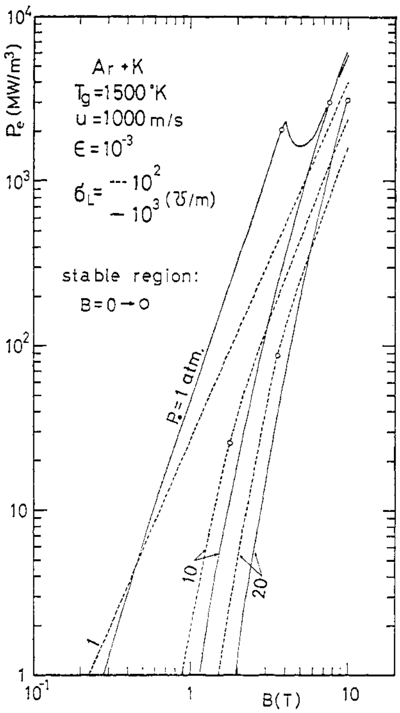

FIG. 18.—Power density vs magnetic field strength for $\varepsilon = 10^{-3}$ and $T_g = 1500$°K for various pressures.

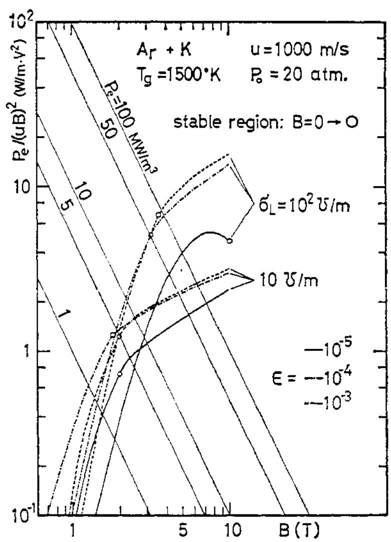

FIG. 19.—$[P_e/(uB)^2]$ vs B at $T_g = 1500$°K and $P_0 = 20$ atm for various seed fractions.

4. CONCLUDING REMARKS

In nonequilibrium MHD generation with potassium seeded argon gas plasma under the conditions of $T_g = 2000°K$ and atmospheric pressure, stable regions free from the ionization instability are very narrowly restricted by the seed fraction, the magnetic field and current density.

It is concluded that in a Faraday-type MHD generator with very finely segmented electrodes the results show the superiority of operations at relatively high seed fractions, for example 10^{-3}, over that at a seed fraction of 10^{-5}, in the region of high magnetic field strengths despite partial ionization of the seed atoms and the occurrence of the ionization instability for $\varepsilon = 10^{-3}$. Furthermore, it turns out that the influence of the operating pressure on the power density of a Faraday-type MHD generator is not pronounced, and that even at a low gas temperature of 1500°K and a pressure of 20 atm, the power density for $\varepsilon = 10^{-3}$ can still reach a value above 50 MW/m^3 for practical values of magnetic field. These results consequently point to the feasibility of closed cycle gas plasma MHD generation operating at a relatively high seed fraction and high pressure.

Acknowledgements—Authors wish to express their thanks to Dr. M. NUMANO for his useful suggestions and discussions, and also to the staff of the Computation Center of Kyoto University.

REFERENCES

BREDERLOW G., FENEBERG W. and HODGSON R. (1966) *Electricity from MHD, Vienna* **2**, 29.
BREDERLOW G. and WITTE K. J. (1973) *Proc. 13th Symp. on Engng. Aspects MHD*, Stanford, I.7.
DETHLEFSEN R. and KERREBROCK J. (1966) *Proc. 7th Symp. on Engng. Aspects MHD*, Princeton, p. 117.
KERREBROCK J. (1964) *AIAA J.* **2**, 1072.
LOUIS J. (1967) *Physics Fluids* **10**, 2062.
NAKAMURA T. and RIEDMÜLLER W. (1971) *Proc. 5th Int. Conf. on MHD Power Generation*, Munich, Vol. 2, p. 291.
NELSON A. and HAINES M. (1969) *Plasma Physics* **11**, 811.
RIEDMÜLLER W. (1973) Rep. IPP, IV/52, Garching.
SOLBES A. (1968) *Electricity from MHD, Vienna* **1**, 499.